

Impact of Thickness of Polymer Electrolyte Membrane and Gas Diffusion Layer on Temperature Distributions in Polymer Electrolyte Fuel Cell Operated at Temperature around 90 °C

Akira Nishimura¹, Yusuke Sato¹, Satoru Kamiya¹, Tatsuya Okado¹, Kouhei Yamamoto¹, Masafumi Hirota¹ and Eric Hu²

1. Division of Mechanical Engineering, Graduate School of Engineering, Mie University, Tsu-city, Mie 514-8507, Japan

2. School of Mechanical Engineering, the University of Adelaide, Adelaide, SA 5005, Australia

Abstract: Polymer Electrolyte Fuel Cell (PEFC) is desired to be operated at temperature around 90 °C for stationary applications during the period from 2020 to 2025 in Japan. It can be expected thinner polymer electrolyte membrane (PEM) and gas diffusion layer (GDL) would promote the power generation performance of PEFC at this temperature. The aim of this study is to understand the impact of thickness of PEM and GDL on the temperature profile of interface between PEM and catalyst layer at the cathode (i.e., the reaction surface) in a single PEFC with an initial operation temperature (T_{ini}). An 1D multi-plate heat transfer model based on temperature data of separator measured using thermograph in power generation process was developed to evaluate temperature of the reaction surface (T_{react}). This study investigated the effect of T_{ini} , flow rate and relative humidity of supply gas on T_{react} distribution. The study finds that when using thin GDL, the even distribution of $T_{react} - T_{ini}$ is obtained irrespective of thickness of PEM, T_{ini} and relative humidity conditions. $T_{react} - T_{ini}$ using Nafion 115 is higher than the other thin PEMs irrespective of T_{ini} and relative humidity conditions. It can be concluded that the even temperature distribution could be achieved by using thin PEM and GDL.

Key words: PEFC, heat transfer model, temperature distribution, operation temperature around 90 °C, thickness of PEM and GDL, relative humidity condition.

1. Introduction

According to NEDO road map 2017 in Japan [1], polymer electrolyte fuel cell (PEFC) is desired to be operated at around 90 °C for stationary applications during the period from 2020 to 2025. However, the current PEFC has Nafion membrane and is usually operated within the temperature range between 60 °C and 80 °C [2, 3]. In this study, the difference between high temperature operation condition and normal condition is the target temperature in the future to the present operation temperature. When PEFC is operated

at high temperature, the following merits can present: (1) enhancement of electrochemical kinetics for both electrode reactions; (2) simplification in the cooling system due to increase in temperature gradient between the PEFC stack and coolant for vehicle use; (3) increase in tolerability of CO and allowing the PEFC to use lower quality reformed hydrogen [4]. In order to develop the PEFC system that could be operated at temperature around 90 °C, its heat and mass transfer characteristics in the power generation process and system durability should be understood, which is the aim of this study. The uneven temperature distribution especially at operation temperature around 90 °C would cause degradations of polymer electrolyte membrane (PEM) and catalyst layer since they are easy

Corresponding author: Akira Nishimura, Ph.D., associate professor, research fields: heat transfer, fuel cell, photocatalyst and smart city.

to be dried. In addition, the temperature distribution also influences the phase change of water. Water's behaviour influences the performance of the PEM, gas flows in gas diffusion layer (GDL) and catalyst layer. Therefore, it is important to understand the temperature distribution in single cell of PEFC in order to improve the power generation performance and realize the long life span, which the aim of this study.

The characteristics of PEFC up to 200 °C were reported [5-28]. However, most of them focused on development of new material [6, 9, 10, 13, 14, 18, 23, 24, 27], the power generation performance such as current density distribution, voltage change [5, 8, 12, 15-17, 21, 22, 25, 26], and durability [7, 11]. A few researches reported the temperature distribution in the single cell of PEFC operated at high temperature [19, 20, 28]. However, they did not investigate the temperature near the interface between PEM and catalyst layer at the cathode, which is termed as a reaction surface in the present paper. Therefore, the heat and mass transfer characteristics of PEFC, which dominates the power generation performance, operated at temperature around 90 °C are not clarified yet.

In the study conducted by Nishimura, et al. [29], the temperature distributions on separator's back of single cell of PEFC were measured by thermograph. The temperature distribution under power generation conditions could be measured accurately since there was no disturbance of heat and mass transfer because of non-destruction measurement. An empirical model to predict the temperature distribution on reaction surface was developed using the measured data. According to the literature survey, there was no precious study to estimate the temperature distribution on reaction surface from measured temperature data at separator's back. If a heat transfer model which can predict the temperature distribution on reaction surface with the measured separator back's temperature would be developed, the temperature distribution could be estimated easily without difficult and complex temperature measurement in future.

According to the studies conducted by Nishimura et al. [30-32], an 1D multi-plate heat transfer model using the temperature data of separator's back measured by thermograph under power generation was developed in order to estimate the temperature distribution inside single cell of PEFC. Since the single cell of PEFC consists of some components having plate shapes such as PEM, catalyst layer, GDL and separator, Nishimura et al. [30-32] proposed the heat transfer model assuming the heat transfer through multi-plates for these components of the cell. The reaction surface temperature (T_{react}) was calculated using the heat transfer model. This is a new approach to identify the heat transfer mechanism in single cell of PEFC by means of the data measured by the thermograph and the model developed. There were the differences between the results from this model [30-32] and the other heat transfer models [33-35]. For example, the 1D model developed by Khandelwal and Mench [33] considers the heat transfer from the PEM, catalyst layer, anode/cathode diffusion media, and backing plate based on Fourier's thermal conduction equation, while this model uses the heat sources such as the Joule heating from the PEM, entropic loss, activation and concentration over-potential, and Joule heating in the catalyst layer. However, the temperature gradients for the targeted regions under the similar operation conditions were almost the same [30]. In addition, the author [36] had already investigated 3D model using commercial CFD software to predict the distribution of T_{react} . This 3D model calculated the equations such as conservation equations of mass, momentum and energy in porous region as well as electrochemical reaction. Comparing the results predicted by the 3D model with that by the 1D model proposed in this study under the several operation conditions, the differences of T_{react} between two models were from 0.1 K to 1.5 K. Therefore, this study thinks that the 1D model proposed in this study has been validated by the 3D model. Thus, it can be believed that, the heat transfer model proposed in the present study is reasonable. In

addition, the advantages of 1D model proposed by this study are considered as follows: (1) The proposed 1D model can predict the temperature distribution on reaction surface without complex simulation using 3D model and temperature measurement with high accuracy. (2) The proposed 1D model can propose the new procedure predicting the temperature distribution on reaction surface using the measured temperature data of separator back without disturbing the heat and mass transfer phenomena as well as power generation characteristics in PEM, catalyst layer and GDL. (3) We can save the time to clarify the mechanism of PEFC and develop PEFC because of simple model.

The aim of the present paper is to develop and validate a heat transfer model to predict the temperature distribution on the reaction surface as well as to clarify the desirable operation condition under operation temperature around 90 °C condition. This study focuses on the thickness of PEM and GDL in order to clarify the desirable operation condition under higher temperature operation especially. Penga et al. [37] reported that the thin PEM whose thickness was 10 μm provided lower ohmic resistance as well as better hydration of the anode H_2 due to increased back diffusion when operated at 60 °C. It can be expected that these positive effects of thinner PEM would promote the power generation performance of PEFC in a higher temperature operation. Comparing the water distribution in GDL whose thickness was 420 μm with that in GDL whose thickness was 235 μm , it was found the thinner GDL has a more abrupt transition of bulk flow as which, pulls water from the catalyst layer and MPL more effectively [38]. In addition, the thin GDL had a more similar water distribution between lands and channels than the thick GDL [38]. Therefore, it can be expected that these positive effects of thinner GDL would promote the power generation performance of PEFC under higher temperature operation. This study evaluates three types of PEM and two types of GDL to investigate the impact of their thickness on temperature distribution on reaction surface. In addition, this study

investigates the effects of initial operation temperature (T_{ini}), flow rate, relative humidity of supply gas on temperature distribution on reaction surface.

2. Calculation Procedures

2.1 1D Multi-plate Heat Transfer Model

Fig. 1 illustrates the multi-plate single cell PEFC module used in this study and in the study [39]. In the module, the separator's back is the opposite side of surface contacting GDL. The separator's back surface temperatures $T_{\text{surf, c}}$ and $T_{\text{surf, a}}$ were measured by using thermograph. The separator which had 5 flow serpentine channels was used to be the objective of thermograph [29] in the power generation process in order to obtain the temperature data.

The heat transfer across the module is assumed to be in 1D direction only. In the module, the cell is divided into a gas channel and a rib part. In Fig. 1, the upper and the lower parts represent rib part and channel part, respectively. For both parts, the heat transfer was assumed to be in the through-plane direction. The reaction heat generated on reaction surface is transferred to the cathode and anode sides separately. Although the gas flowing through the gas channel from the inlet to the outlet of the cell carries away some heat, the amount of heat taken is less than 1% of the estimated reaction heat of approximately 20 W [30]. Therefore, the heat carried away by the gas flow was neglected in this model. Additionally, the mass flow rate of gas flowing through the gas channel is very small ranging from 10^{-8} to 10^{-6} kg/s, resulting that the thermal conduction of gas in the gas channel is assumed since the gas is thought to be static. In addition, in the model propose by this study, the heat pipe effect due to phase change of water is not considered. However, it was reported that the temperature difference between T_{react} under the rib and that under the channel is small, which is approximately within 1 K at 70–80 °C, according to the other studies conducting the numerical simulation by 3D model considering phase change of water [40, 41].

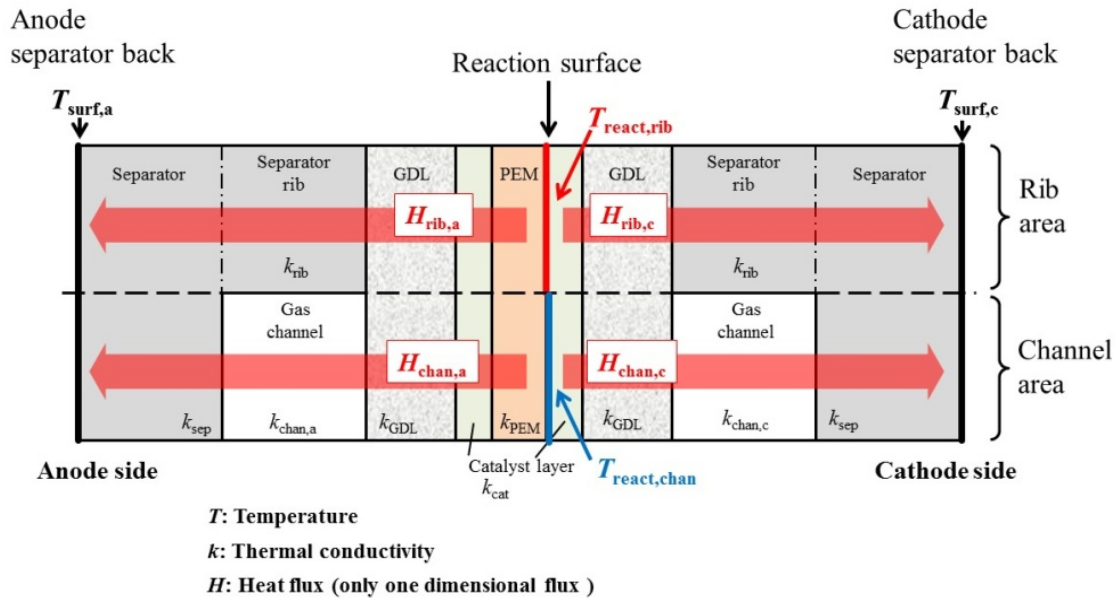


Fig. 1 1D multi-plate heat transfer module.

Therefore, this study thinks that the heat pipe effect assists heat removal under the channel is small.

2.2 Reaction Heat Generation Rate

The reaction heat generation rate H_{react} is calculated as the follows [32, 39]:

$$H_{\text{react}} = E_i - W_E \quad (1)$$

where, E_i is the ideal (total) energy generation rate by the water formation from H_2 and O_2 based on higher heating value except $T_{\text{ini}} = 100$ °C. The lower heating value is adopted for $T_{\text{ini}} = 100$ °C. W_E is the electric work generated by PEFC. E_i and W_E are expressed as follows:

$$E_i = m_{H_2} \times q_{\text{HHV}} \text{ or } q_{\text{LHV}} \quad (2)$$

$$W_E = I \times V \quad (3)$$

where, I is the total current obtained by the experiment (= 20 A) excluding some operation conditions. In this study, the power generation data setting a load current at 20 A (= 0.80 A·cm²) were used for the heat transfer modeling. V is the voltage obtained by the experiment. m_{H_2} is the molar flow rate of supplied H_2 , which is equal to the ideal reaction consumption rate of H_2 required for the generation at 20 A, i.e., the stoichiometric ratio (s.r.) of 1.0. Here, s.r. is the ratio of the feed amount of H_2 or O_2 to that required to generate

a current of 20 A. The flow rate of supply gas (H_2) at s.r. of 1.0 is defined as follows:

$$m_{H_2} = I/nF \quad (4)$$

where, m_{H_2} is the molar flow rate of supplied H_2 (mol·s⁻¹); n is the valence of ion (= 2 for H_2); F is the Faraday constant (= 96,500 C·mol⁻¹). m_{O_2} which is the molar flow rate of supplied O_2 (mol·s⁻¹) and is calculated as follows:



The actual s.r. of supply gas was confirmed, using the mass flow controller installed at the inlet of the single cell and the mass flow meter installed at the outlet of the cell in the power generation experiment [29].

2.3 Heat-Balance Equations for Calculating Reaction Surface Temperature [39]

The heats transferred in the model proposed are expressed as Eqs. (6)-(10):

$$H_{\text{rib, c}} = K_{\text{rib, c}} A (T_{\text{react, rib}} - T_{\text{surf, c}})/2 \quad (6)$$

$$H_{\text{chan, c}} = K_{\text{chan, c}} A (T_{\text{react, chan}} - T_{\text{surf, c}})/2 \quad (7)$$

$$H_{\text{rib, a}} = K_{\text{rib, a}} A (T_{\text{react, rib}} - T_{\text{surf, a}})/2 \quad (8)$$

$$H_{\text{chan, a}} = K_{\text{chan, a}} A (T_{\text{react, chan}} - T_{\text{surf, a}})/2 \quad (9)$$

$$H_{\text{react}} = H_{\text{rib, c}} + H_{\text{chan, c}} + H_{\text{rib, a}} + H_{\text{chan, a}} \quad (10)$$

where, $H_{\text{rib, c}}$ is the heat flux to cathode side under rib

(W); $K_{rib, c}$ is the overall heat transfer coefficient for cathode side under rib ($W \cdot m^{-2} \cdot K^{-1}$); A is the heat transfer area which is the active area of MEA, i.e., power generation area ($= 0.0025 \text{ m}^2$); $T_{react, rib}$ is the reaction surface temperature under rib (K or °C); $T_{surf, c}$ is the separator's back surface temperature at cathode (K or °C); $H_{chan, c}$ is the heat flux to cathode side under channel (W); $K_{chan, c}$ is the overall heat transfer coefficient for cathode side under channel ($W \cdot m^{-2} \cdot K^{-1}$); $T_{react, chan}$ is the reaction surface temperature under channel (K or °C); $H_{rib, a}$ is the heat flux to anode side under rib (W); $K_{rib, a}$ is the overall heat transfer coefficient for anode side under rib ($W \cdot m^{-2} \cdot K^{-1}$); $T_{surf, a}$ is the separator's back temperature at anode (K or °C); $H_{chan, a}$ is the heat flux to anode side under channel (W); $K_{chan, a}$ is the overall heat transfer coefficient for anode side under channel ($W \cdot m^{-2} \cdot K^{-1}$). $K_{rib, c}$, $K_{chan, c}$, $K_{rib, a}$ and $K_{chan, a}$ are defined as follows:

$$1/K_{rib, c} = \delta_{cat}/k_{cat} + \delta_{GDL}/k_{GDL} + \delta_{rib}/k_{rib} + \delta_{sep}/k_{sep} \quad (11)$$

$$1/K_{chan, c} = \delta_{cat}/k_{cat} + \delta_{GDL}/k_{GDL} + \delta_{chan}/k_{chan, c} + \delta_{sep}/k_{sep} \quad (12)$$

$$1/K_{rib, a} = \delta_{PEM}/k_{PEM} + \delta_{cat}/k_{cat} + \delta_{GDL}/k_{GDL} + \delta_{rib}/k_{rib} + \delta_{sep}/k_{sep} \quad (13)$$

$$1/K_{chan, a} = \delta_{PEM}/k_{PEM} + \delta_{cat}/k_{cat} + \delta_{GDL}/k_{GDL} + \delta_{chan}/k_{chan, a} + \delta_{sep}/k_{sep} \quad (14)$$

where, δ_{cat} is the thickness of the catalyst layer (m); k_{cat} is the thermal conductivity of the catalyst layer ($W \cdot m^{-1} \cdot K^{-1}$); δ_{GDL} is the thickness of GDL (m); k_{GDL} is the thermal conductivity of GDL ($W \cdot m^{-1} \cdot K^{-1}$); δ_{rib} is the thickness of the separator rib (m); k_{rib} is the thermal conductivity of the separator rib ($W \cdot m^{-1} \cdot K^{-1}$); δ_{sep} is the thickness of the separator excluding rib part (m); k_{sep} is the thermal conductivity of the separator excluding rib part ($W \cdot m^{-1} \cdot K^{-1}$); δ_{chan} is the thickness of the channel of separator (m); k_{chan} is the thermal conductivity of the mixture gas in the channel of separator ($W \cdot m^{-1} \cdot K^{-1}$); δ_{PEM} is the thickness of PEM (m); k_{PEM} is the thermal conductivity of PEM ($W \cdot m^{-1} \cdot K^{-1}$).

Table 1 lists the specification of cell components used in the model. Nafion 115, NRE-212 and NRE-211

(proposed by Du Pont Corp.) whose thicknesses are 127 μm , 51 μm and 25 μm , respectively, are evaluated. In addition, TGP-H-060 and TGP-H-030 (produced by Toray Corp.) whose thicknesses are 190 μm and 110 μm , respectively, are evaluated. The model consists of PEM, catalyst layer, GDL and separator. The thickness values listed here are the same as those of the components used by previous studies [29, 37-39].

In Table 1, the effective thermal conductivities of porous media k , are the values of the cell components used in the present experiment and in Refs. [29, 33]. Since the effective thermal conductivities given in Table 1 are obtained when the cell component pores are filled with air at room temperature, the corrected effective thermal conductivities are calculated for the cell component pores filled with H_2 or O_2 at 80 °C or 90 °C, which are the T_{ini} value assumed in this study. In this calculation, the thermal conductivities of each gas are from The Japan Society of Mechanical Engineers [42].

In order to solve Eqs. (6)-(9), the temperatures measured using the thermograph were substituted into these equations as $T_{surf, c}$ and $T_{surf, a}$. The operation conditions used for power generation in order to measure temperatures with thermograph are given in Table 2. Analysis using 1D multi-plate heat transfer is carried out by means of the data obtained under these conditions. In the power generation process in order to obtain the temperature data by thermograph, the current density was kept at 0.80 $A \cdot cm^{-2}$, so the cell temperature could be kept higher than the initial temperature with no heat input from the electric heater required [29, 42]. Therefore, the temperature distribution data caused by reaction heat only at separator back could be obtained. The experimental procedure for measuring temperature during power generation has been explained in Refs. [29, 40].

In order to use the temperature data measured by thermograph in 1D multi-plate heat transfer model, the image of in-plane temperature distribution is divided into segments of 10 mm \times 10 mm each, as shown in

Table 1 Specification of PEFC components referred from the manufacture catalog and previous studies [29, 37-39].

Parts	Size	Characteristics	Porosity (-)	Effective thermal conductivity ($W \cdot m^{-1} \cdot K^{-1}$)
Polymer electrolyte membrane (PEM)	50.0 mm × 50.0 mm × 0.127 mm (Nafion 115), 50.0 mm × 50.0 mm × 0.051 mm (NRE-212) or 50.0 mm × 50.0 mm × 0.025 mm (NRE-211)	Nafion 115, NRE-212 or NRE-211 (produced by Du Pont Corp.)	0.28	0.195
Catalyst layer	50.0 mm × 50.0 mm × 0.01 mm (attached with PEM)	Pt/C (20 wt% Pt loading)	0.78	0.27
Gas diffusion layer (GDL)	50.0 mm × 50.0 mm × 0.19 mm (TGP-H-060) or 50.0 mm × 50.0 mm × 0.11 mm (TGP-H-030)	Carbon paper (TGP-H-060 produced by Toray Corp.)	0.78 (TGP-H-060), 0.80 (TGP-H-030)	1.7
Separator	75.4 mm × 75.4 mm × 2.00 mm (thickness of rib part: 1.00 mm) (Gas supply area: 50.0 mm × 50.0 mm)	Carbon graphite, serpentine	0.15	25

Table 2 Operating conditions of power generation for temperature measurement by thermograph.

Initial temperature of cell (T_{ini}) (°C)	80, 90, 100	
Load current of cell (A) (current density of cell ($A \cdot cm^{-2}$))	20 (0.80)	
	Supply gas condition	
	Anode	Cathode
Gas type	H_2	O_2
Temperature of supply gas at inlet (°C)	80, 90, 100	80, 90, 100
Relative humidity of supply gas (% RH)	40, 80	40, 80
Pressure of supply gas at inlet (absolute) (MPa)	0.4	0.4
Flow rate of supply gas at inlet ($NL \cdot min^{-1}$) (Stoichiometric ratio (-))	0.210 (1.5), 0.280 (2.0), 0.420 (3.0)	0.105 (1.5), 0.140 (2.0), 0.210 (3.0)

Fig. 2. Although the power generation area is 50 mm × 50 mm, the observation area is set to be 40 mm × 50 mm to prevent a gas leak through observation window in the experiments. The gas channel width and the rib width of investigated separator are 1.0 mm and the number of gas channel is 5. The segment includes the area consisting of five pairs of rib and gas channel. The average temperature in each segment at anode and cathode was used for the separator's back temperature in 1D multi-plate heat transfer model. The segment is named A to T along the gas flow direction as shown in Fig. 2.

Regarding segments A and T, the insulators covering the gas pipes interfere with the thermograph measurement in some area of the segment as it can be seen in Fig. 2. In this study, the effective temperature of segments A and T was obtained by

removing the temperature data that were interfered by the insulator from the total temperature data in each segment. In the heat transfer analysis, it was assumed that $T_{surf, c}$ on the rib side was equal to $T_{surf, c}$ on the channel side as well as $T_{surf, a}$ because the difference between them could not be recognized by the measured data.

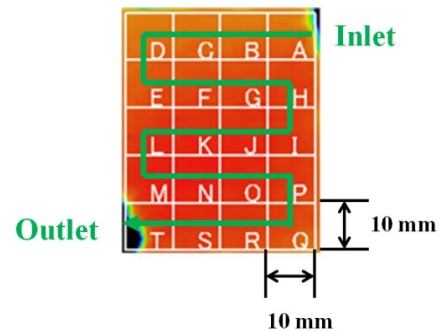


Fig. 2 Segment display of in-plane temperature distribution measured by thermograph.

Considering the above described assumptions and Eqs. (6)-(14), the reaction surface temperature T_{react} is expressed as follows:

$$T_{\text{react}} = T_{\text{react, rib}} = T_{\text{react, chan}} = \{2H_{\text{react}}/A + (K_{\text{rib, c}} + K_{\text{chan, c}})/T_{\text{surf, c}} + (K_{\text{rib, a}} + K_{\text{chan, a}})T_{\text{surf, a}}\} / (K_{\text{rib, c}} + K_{\text{chan, c}} + K_{\text{rib, a}} + K_{\text{chan, a}}) \quad (15)$$

3. Results and Discussion

3.1 Impact of Flow Rate of Supply Gas at Inlet on Temperature Distribution

It is believed that flow rate of supply gas at inlet influences the heat and mass transfer as well as power generation performance from the viewpoint of gas diffusion and water transfer. Fig. 3 shows the impact of stoichiometric ratio (s.r.) of supply gas on temperature distribution on reaction surface simulated by the proposed heat transfer model for Nafion 115 and TGP-H-060. The relative humidity of supply gas is 80% RH at the anode and 80% RH at the cathode (A80%RH, C80%RH). The s.r. of supply gases is 1.5, 2.0 and 3.0. The results obtained at $T_{\text{ini}} = 90 \text{ }^\circ\text{C}$ are shown in these figures.

From Fig. 3, it is observed that $T_{\text{react}} - T_{\text{ini}}$ increases along the gas flow from the inlet to the outlet gradually. Since the PEM is hydrated by the water produced by electrochemical reaction and the humidified gas flows through the outlet, this trend indicates that the power generation is promoted along the gas flow. However, it can also be seen that the impact of flow rate of supply gas at the inlet on the temperature distribution is not significant. The reason could be that the gas supply is sufficient for power generation even s.r. = 1.5. The result confirmed the impact of flow rate of supply gas at the inlet on the temperature distribution is not significant irrespective of relative humidity condition and T_{ini} as well as thickness of PEM and GEL. Since the power generation characteristics obtained by experiment in this study are almost the same among different s.r., the results for s.r. = 1.5 are shown in the following section since they can represent the characteristics of different stoichiometric ratios.

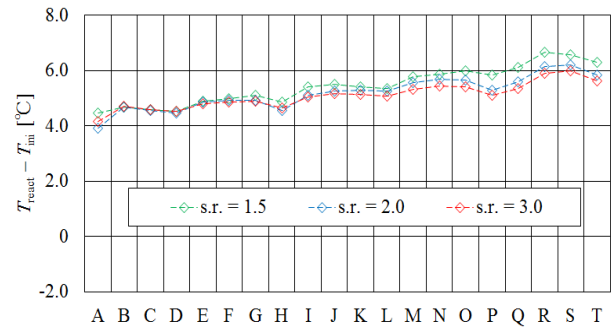


Fig. 3 Effect of stoichiometric ratio of supply gas on distribution of $T_{\text{react}} - T_{\text{ini}}$ at $T_{\text{ini}} = 90 \text{ }^\circ\text{C}$ using Nafion 115 & TGP-H-060 (A80%RH, C80%RH).

3.2 Impact of GDL on Temperature Distribution

Since it is believed that gas diffusion and water discharge are promoted with the decrease in thickness of GDL [38], the impact of thickness of GDL on temperature distribution on reaction surface is investigated in this study. Fig. 4 shows the impact of thickness of GDL on temperature distribution on reaction surface using Nafion 115 for A80%RH, C80%RH at $T_{\text{ini}} = 80 \text{ }^\circ\text{C}$, $90 \text{ }^\circ\text{C}$ and $100 \text{ }^\circ\text{C}$, respectively. To investigate the effect of relative humidity condition at the same time, Fig. 5 shows the impact of thickness of GDL on temperature distribution on reaction surface of Nafion 115 when the relative humidity of supply gas is 80% RH at the anode and 40% RH at the cathode (A80%RH, C40%RH) at $T_{\text{ini}} = 80 \text{ }^\circ\text{C}$, $90 \text{ }^\circ\text{C}$ and $100 \text{ }^\circ\text{C}$, respectively. In addition, Fig. 6 shows the impact of thickness of GDL on temperature distribution on reaction surface when the relative humidity of supply gas is 40% RH at the anode and 80% RH at the cathode (A40%RH, C80%RH) at $T_{\text{ini}} = 80 \text{ }^\circ\text{C}$ and $90 \text{ }^\circ\text{C}$, respectively.

According to Figs. 4-6, it is seen that $T_{\text{react}} - T_{\text{ini}}$ is increased from the inlet to the outlet by $2 \text{ }^\circ\text{C}$ to $3 \text{ }^\circ\text{C}$ when using TGP-H-060, and by $1 \text{ }^\circ\text{C}$ when using TGP-H-030. Since the water discharge performance is weak and liquid water is easy to be accumulated due to the thick TGP-H-060 used, it is thought that the temperature rises along the gas flow caused by condensation heat of accumulating water.

Impact of Thickness of Polymer Electrolyte Membrane and Gas Diffusion Layer on Temperature Distributions in Polymer Electrolyte Fuel Cell Operated at Temperature around 90 °C

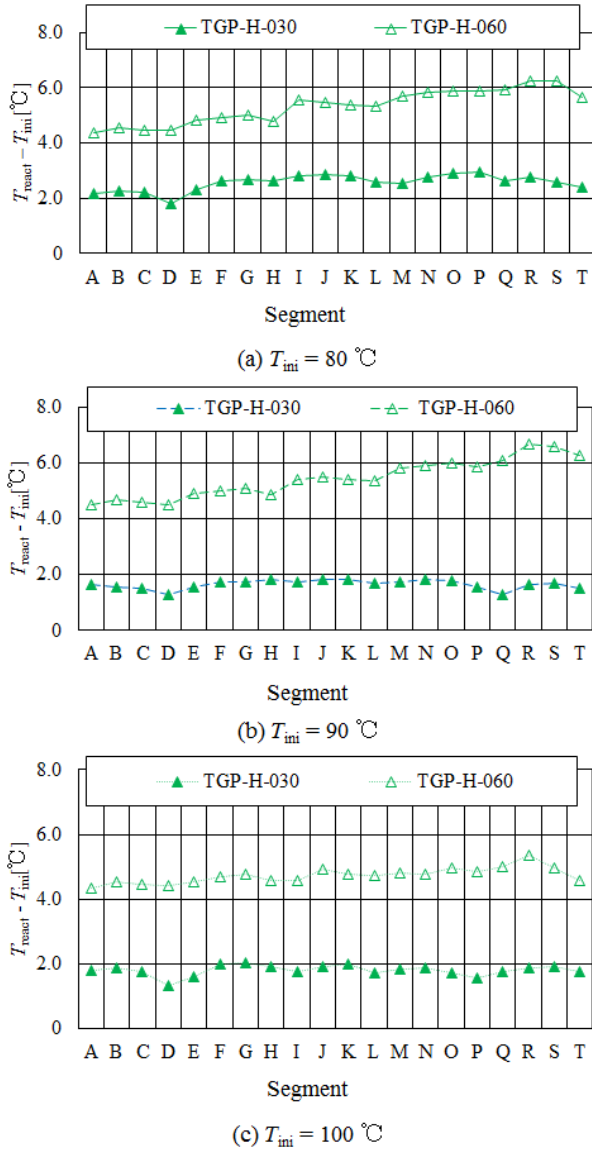


Fig. 4 Effect of thickness of GDL on T_{react} for A80%RH, C80%RH at $T_{\text{ini}} = 80$ °C, 90 °C, 100 °C using Nafion 115.

In addition, it is revealed that the distribution of $T_{\text{react}} - T_{\text{ini}}$ when using TGP-H-030 is nearly flat. When using a thinner GDL, the water discharge performance is better, resulting that the accumulation of liquid water is prevented. Since the gas diffusion is promoted, it is believed that the power generation occurs from the inlet to the outlet uniformly, resulting in the even distribution of $T_{\text{react}} - T_{\text{ini}}$. In addition, the flow resistance when using thin GDL is smaller than that in thick GDL case [43], and temperature distribution becomes even due to high heat transfer rate. For

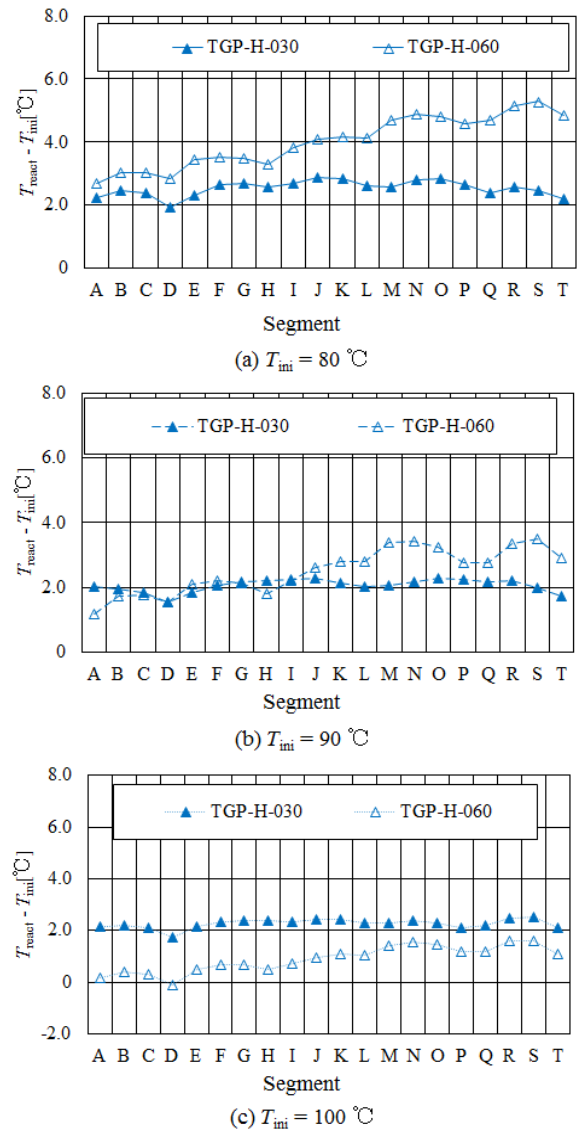
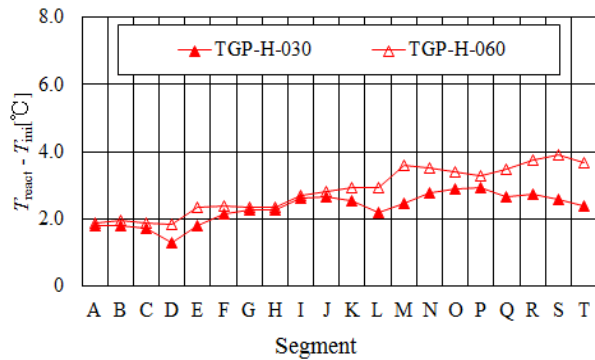
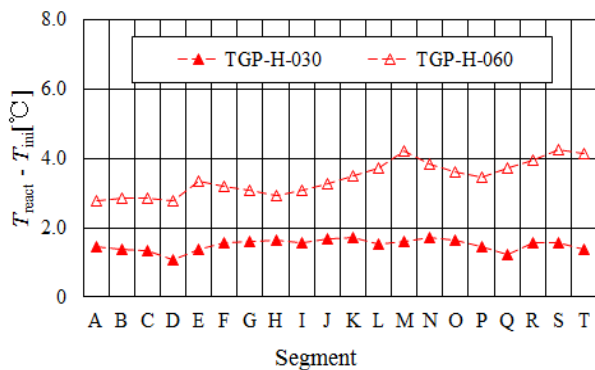


Fig. 5 Effect of thickness of GDL on T_{react} for A80%RH, C40%RH at $T_{\text{ini}} = 80$ °C, 90 °C, 100 °C using Nafion 115.

example, the voltage for A80%RH, C80%RH at $T_{\text{ini}} = 90$ °C using TGP-H-030 which was obtained from the power generation experiment was 0.47 V, while that using TGP-H-060 was 0.46 V. The power generation performance using TGP-H-030 is superior to that using TGP-H-060. This tendency is confirmed under the low relative humidity condition remarkably. The voltage for A80%RH, C40%RH at $T_{\text{ini}} = 90$ °C using TGP-H-030 which was obtained from the power generation experiment was 0.45 V, while that using TGP-H-060 was 0.34 V. In addition, the voltage for



(a) $T_{ini} = 80\text{ }^{\circ}\text{C}$

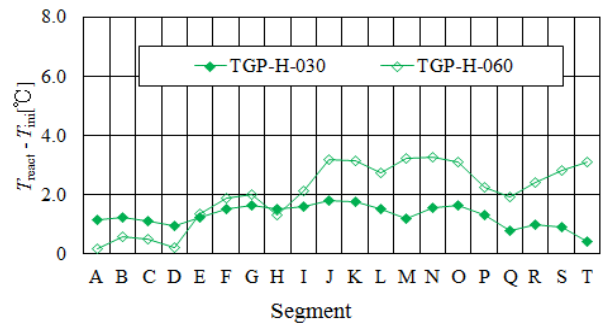


(b) $T_{ini} = 90\text{ }^{\circ}\text{C}$

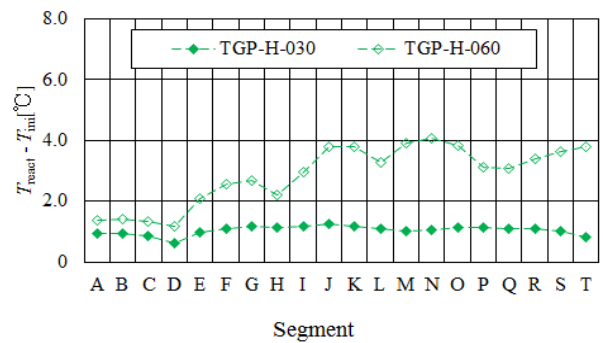
Fig. 6 Effect of thickness of GDL on T_{react} for A40%RH, C80%RH at $T_{ini} = 80\text{ }^{\circ}\text{C}$, $90\text{ }^{\circ}\text{C}$, $100\text{ }^{\circ}\text{C}$ using Nafion 115.

A40%RH, C80%RH at $T_{ini} = 90\text{ }^{\circ}\text{C}$ using TGP-H-030 which was obtained from the power generation experiment was 0.45 V, while that using TGP-H-060 was 0.22 V. From these results, it can conclude that the water transfer from the anode to the cathode or from the cathode to the anode by electro-osmotic drag or back diffusion, respectively, is promoted with the decrease in thickness of GDL due to the increase of gas permeability [44].

Fig. 7 shows the impact of thickness of GDL on temperature distribution on reaction surface of NRE-211 for A80%RH, C80%RH at $T_{ini} = 80\text{ }^{\circ}\text{C}$ and $90\text{ }^{\circ}\text{C}$, while Fig. 8 shows the impact of thickness of GDL on temperature distribution on reaction surface of NRE-211 for A80%RH, C40%RH at $T_{ini} = 80\text{ }^{\circ}\text{C}$ and $90\text{ }^{\circ}\text{C}$. In addition, Fig. 9 shows the impact of thickness of GDL on temperature distribution on reaction surface of NRE-211 for A40%RH, C80%RH at $T_{ini} = 80\text{ }^{\circ}\text{C}$ and $90\text{ }^{\circ}\text{C}$. When using NRE-211, the power generation

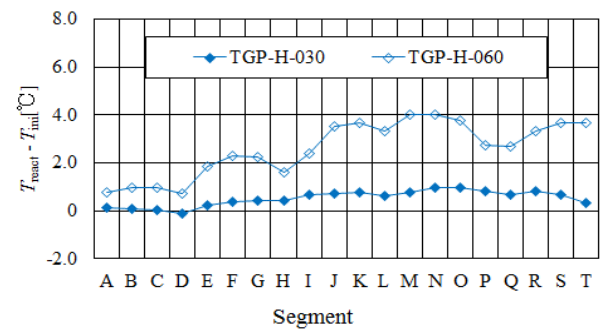


(a) $T_{ini} = 80\text{ }^{\circ}\text{C}$

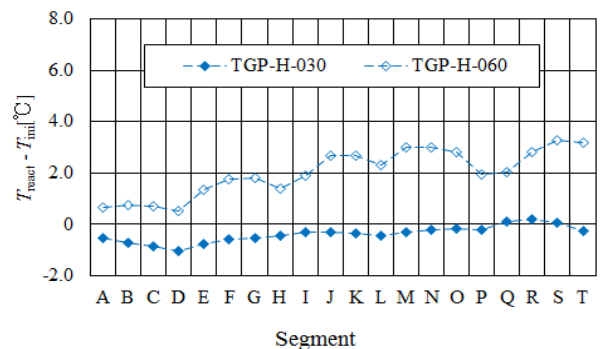


(b) $T_{ini} = 90\text{ }^{\circ}\text{C}$

Fig. 7 Effect of thickness of GDL on T_{react} for A80%RH, C80%RH at $T_{ini} = 80\text{ }^{\circ}\text{C}$, $90\text{ }^{\circ}\text{C}$, $100\text{ }^{\circ}\text{C}$ using NRE-211.



(a) $T_{ini} = 80\text{ }^{\circ}\text{C}$



(b) $T_{ini} = 90\text{ }^{\circ}\text{C}$

Fig. 8 Effect of thickness of GDL on T_{react} for A80%RH, C40%RH at $T_{ini} = 80\text{ }^{\circ}\text{C}$, $90\text{ }^{\circ}\text{C}$, $100\text{ }^{\circ}\text{C}$ using NRE-211.

Impact of Thickness of Polymer Electrolyte Membrane and Gas Diffusion Layer on Temperature Distributions in Polymer Electrolyte Fuel Cell Operated at Temperature around 90 °C

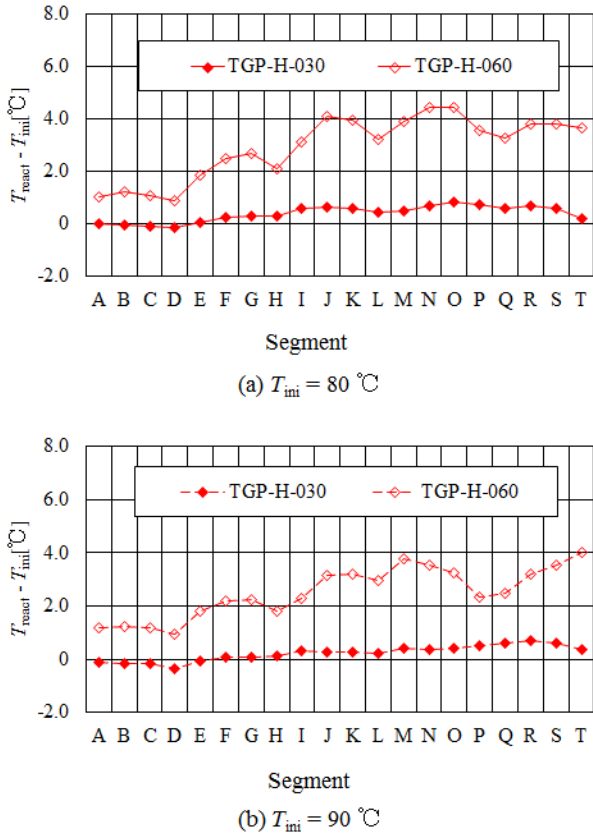


Fig. 9 Effect of thickness of GDL on T_{react} for A40%RH, C80%RH at $T_{\text{ini}} = 80$ °C, 90 °C, 100 °C using NRE-211.

could not be carried out at $T_{\text{ini}} = 100$ °C in the experiment. Therefore, the analysis results at $T_{\text{ini}} = 100$ °C are not shown here.

According to Figs. 7-9, it is seen that $T_{\text{react}} - T_{\text{ini}}$ is increased from the inlet to the outlet by 2 °C to 4 °C when using TGP-H-060, and by 1 °C when using TGP-H-030. This tendency is the same as using thick PEM (Nafion 115). When using thinner GDL, the water discharge performance is better irrespective of thickness of PEM, resulting that the accumulation of liquid water is prevented. Since the gas diffusion is promoted, it is believed that the power is generated from the inlet to the outlet uniformly, resulting in the even distribution of $T_{\text{react}} - T_{\text{ini}}$. Consequently, the thin GDL is more effective for controlling the heat and mass transfer than thick GDL. In the next section, the impact of thickness of PEM on temperature distribution on reaction surface is investigated when using a thin GDL.

Measured T_{surf} with $T_{\text{ini}} = 90$ °C which is the target temperature in this study gives the tendency of base data. Fig. 10 shows $T_{\text{surf, a}}$ and $T_{\text{surf, c}}$ under different relative humidity conditions all with $T_{\text{ini}} = 90$ °C using Nafion 115 and TGP-H-030. Fig. 11 shows that using NRE-212 and TGP-H-030. Fig. 12 shows that using NRE-211 and TGP-H-030. Fig. 13 shows that using Nafion 115 and TGP-H-060. Figs. 14 and 15 show $T_{\text{surf, a}}$ and $T_{\text{surf, c}}$ using NRE-212 and TGP-H-060, using NRE-211 and TGP-H-060, respectively. The all data in Figs. 10-15 were obtained when the stoichiometric ratio of supply gas at inlet was 1.5.

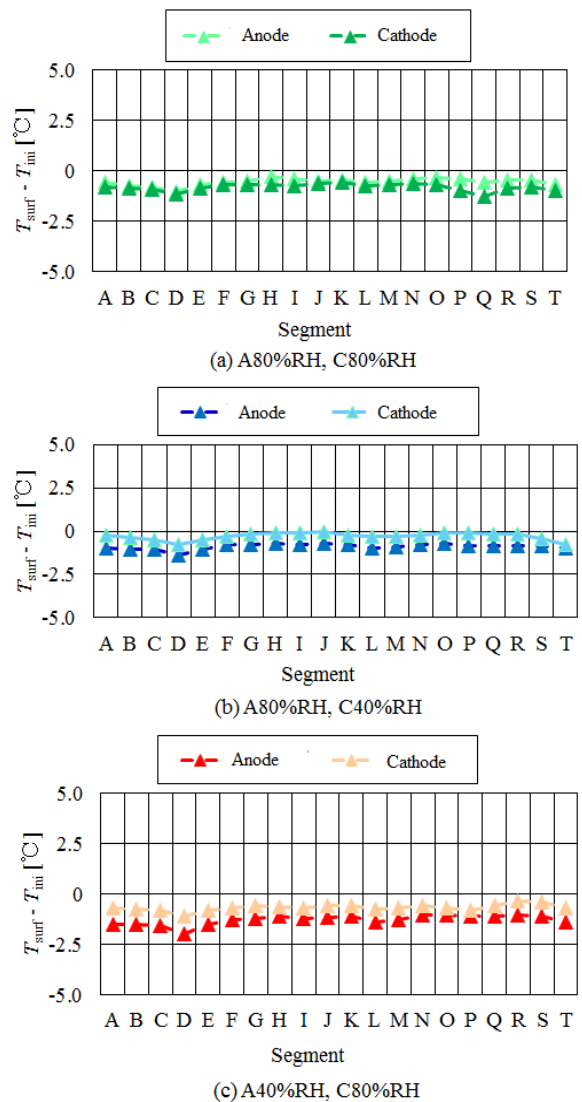
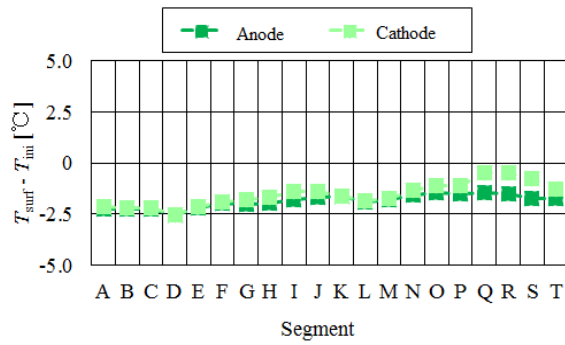
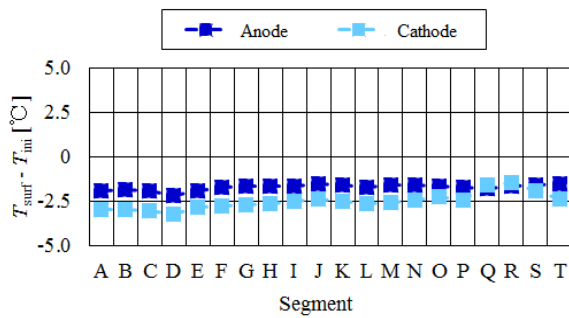


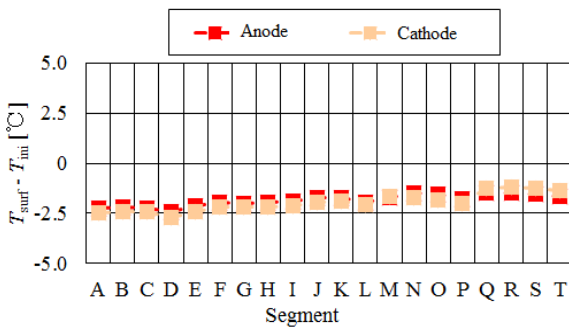
Fig. 10 Comparison of T_{surf} under different relative humidity conditions at $T_{\text{ini}} = 90$ °C using Nafion 115 and TGP-H-030.



(a) A80%RH, C80%RH



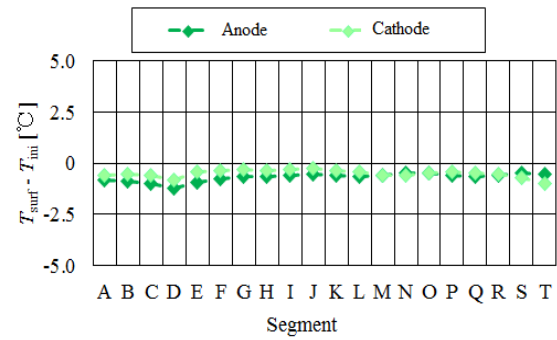
(b) A80%RH, C40%RH



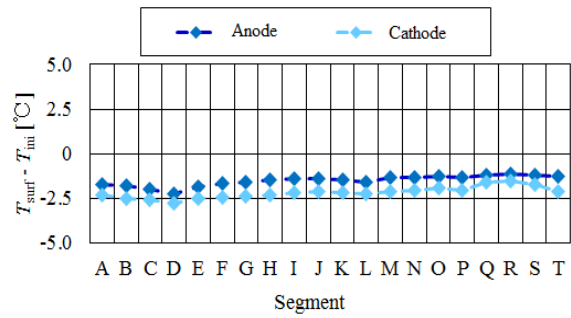
(c) A40%RH, C80%RH

Fig. 11 Comparison of T_{surf} under different relative humidity conditions at $T_{ini} = 90$ °C using NRE-212 and TGP-H-030.

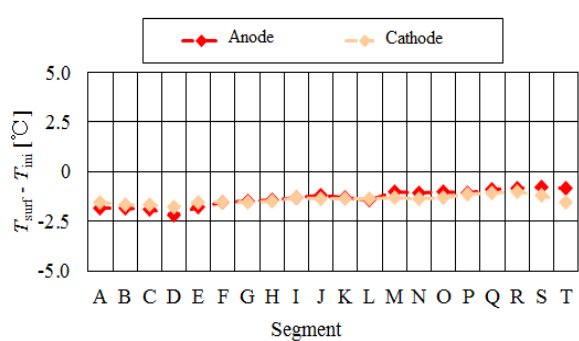
According to these figures, the difference between $T_{surf, a}$ and $T_{surf, c}$ is larger when using thick GDL, i.e., TGP-H-060, while it is small when using thin GDL, i.e., TGP-H-030. Especially, it is revealed that the difference between $T_{surf, a}$ and $T_{surf, c}$ is the largest when using the combination of thick PEM and GDL, i.e., Nafion 115 and TGP-H-060. The reason is thought to be that when using thick GDL and PEM, the heat transfer in through-plane direction is worse due to increase in thickness. In addition, it can be observed that $T_{surf} - T_{ini}$ increases along the flow direction



(a) A80%RH, C80%RH



(b) A80%RH, C40%RH



(c) A40%RH, C80%RH

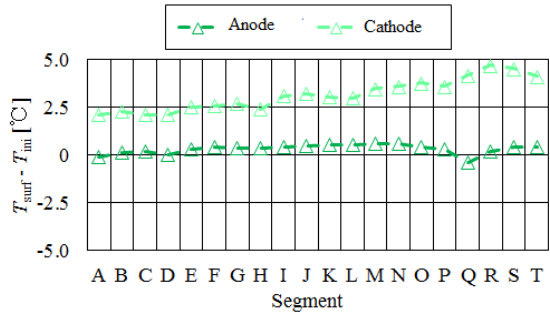
Fig. 12 Comparison of T_{surf} under different relative humidity conditions at $T_{ini} = 90$ °C using NRE-211 and TGP-H-030.

gradually when using TGP-H-060. The same tendency for $T_{react} - T_{ini}$ can also be observed.

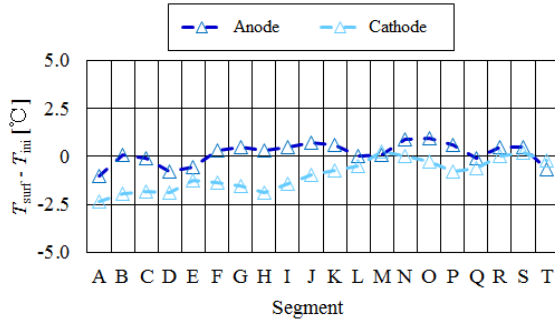
3.3 Impact of PEM on Temperature Distribution

Since it is believed that proton and water transfer is promoted with the decrease in the thickness of PEM [37], the impact of thickness of PEM on temperature distribution on reaction surface is investigated in this study. Fig. 16 shows the impact of thickness of PEM on temperature distribution on reaction surface when using TGP-H-030 with A80%RH, C80%RH at

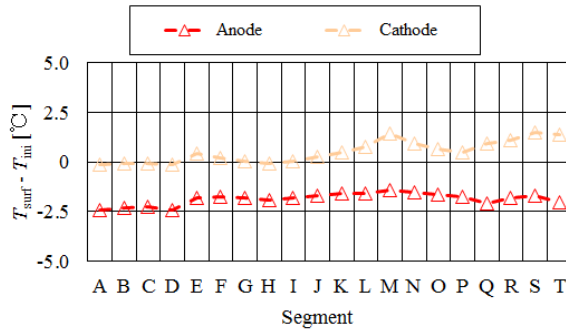
Impact of Thickness of Polymer Electrolyte Membrane and Gas Diffusion Layer on Temperature Distributions in Polymer Electrolyte Fuel Cell Operated at Temperature around 90 °C



(a) A80%RH, C80%RH



(b) A80%RH, C40%RH

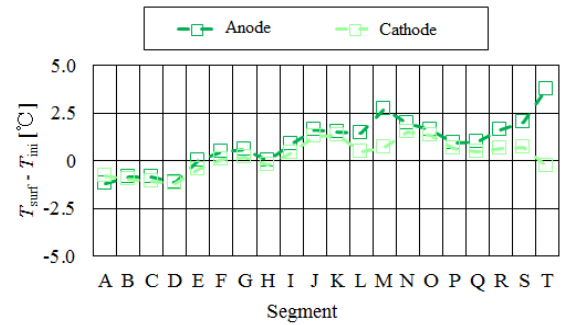


(c) A40%RH, C80%RH

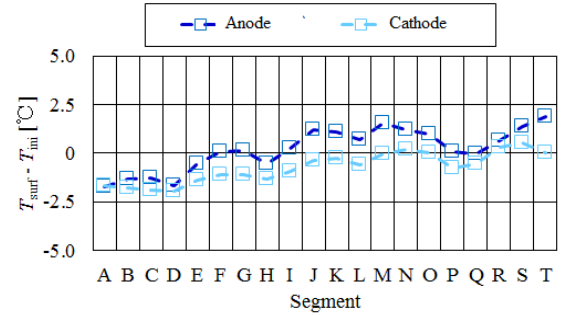
Fig. 13 Comparison of T_{surf} under different relative humidity conditions at $T_{ini} = 90$ °C using Nafion 115 and TGP-H-060.

$T_{ini} = 80$ °C, 90 °C and 100 °C, respectively. Fig. 17 shows the impact of thickness of PEM on temperature distribution on reaction surface when using TGP-H-030 with A80%RH, C40%RH at $T_{ini} = 80$ °C, 90 °C and 100 °C, respectively. In addition, Fig. 18 shows the impact of thickness of PEM on temperature distribution on reaction surface when using TGP-H-030 with A40%RH, C80%RH at $T_{ini} = 80$ °C, 90 °C and 100 °C, respectively.

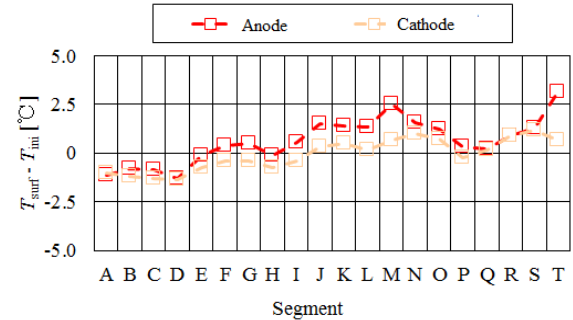
According to Figs. 16-18, it is clear that $T_{react} - T_{ini}$ using Nafion 115 is higher than the other PEMs irrespective of T_{ini} and relative humidity conditions.



(a) A80%RH, C80%RH



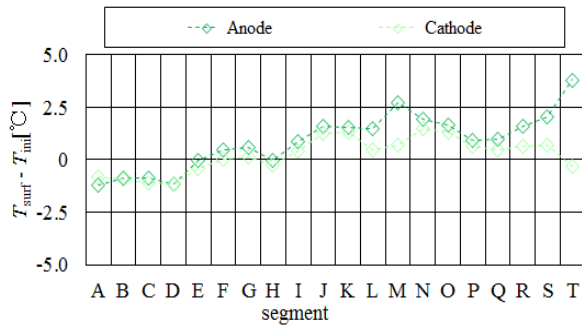
(b) A80%RH, C40%RH



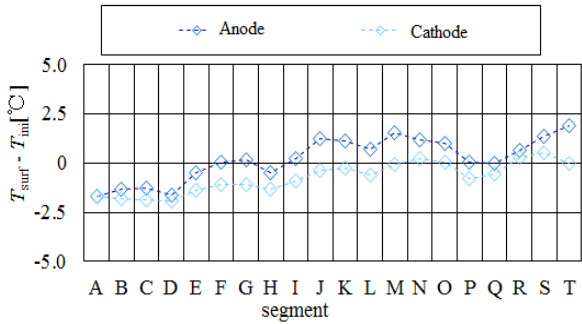
(c) A40%RH, C80%RH

Fig. 14 Comparison of T_{surf} under different relative humidity conditions at $T_{ini} = 90$ °C using NRE-212 and TGP-H-060.

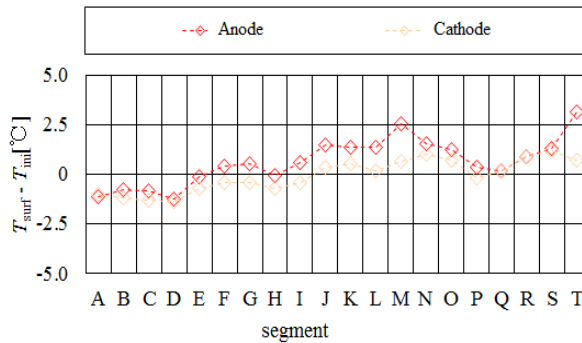
Since the thickness of Nafion 115 is the thickest among investigated PEMs, it is believed that the proton and water transfer is the worst among them [37]. Therefore, the power generation performance using Nafion 115 is also the worst which is shown in Table 3 and Figs. 19-21. It is known from Eqs. (1)-(3) that H_{react} is higher when W_E , i.e., the power generation performance, is smaller, resulting that T_{react} is higher according to Eq. (15). In addition, another reason might be that the condensation heat of accumulated water also contributed to the rise of the temperature.



(a) A80%RH, C80%RH



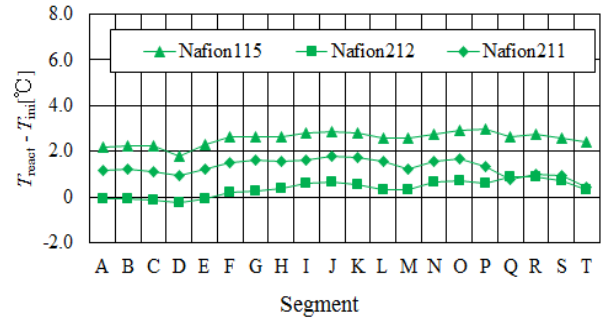
(b) A80%RH, C40%RH



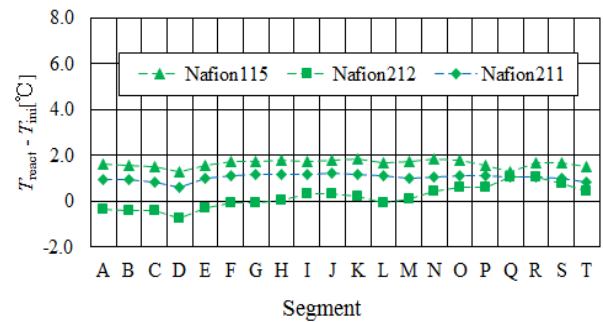
(c) A40%RH, C80%RH

Fig. 15 Comparison of T_{surf} under different relative humidity conditions at $T_{ini} = 90\text{ °C}$ using NRE-211 and TGP-H-060.

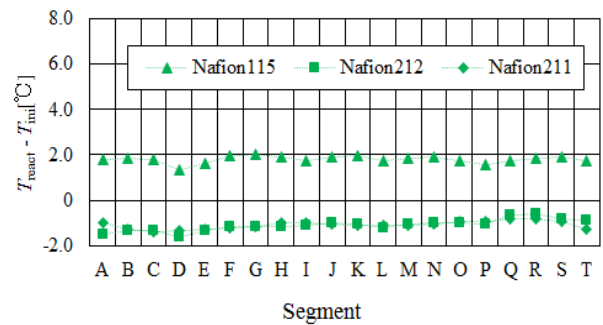
On the other hand, it can be seen that the difference between the distribution of $T_{react} - T_{ini}$ using NRE-212 and that using NRE-211 is small except for A80%RH, C80%RH at $T_{ini} = 80\text{ °C}$ and 90 °C . It is believed that water transfer is good with both NRE-212 and NRE-211 under low relative humidity or high operation temperature, e.g., 90 °C and 100 °C , which results that the difference of the distribution of $T_{react} - T_{in}$ is not recognized well. However, it might be thought that the difference of water transfer between NRE-212 and NRE-211 due to the difference of thickness is larger under high relative humidity



(a) $T_{ini} = 80\text{ °C}$



(b) $T_{ini} = 90\text{ °C}$



(c) $T_{ini} = 100\text{ °C}$

Fig. 16 Effect of thickness of PEM on T_{react} for A80%RH, C80%RH at $T_{ini} = 80\text{ °C}$, 90 °C , 100 °C using TGP-H-030.

condition since liquid water is easy to be produced. Therefore, the difference between the distribution of $T_{react} - T_{ini}$ using NRE-212 and that using NRE-211 is relatively large for A80%RH, C80%RH at $T_{ini} = 80\text{ °C}$ and 90 °C . In other words, it can be claimed that $T_{react} - T_{ini}$ is increased from the inlet to the outlet using NRE-212, which is the same as the case using TGP-H-060 as shown before, due to the bad water transfer performance relatively.

According to Figs. 16-18, it is clear that $T_{react} - T_{ini}$ using Nafion 115 is higher than the other PEMs irrespective of T_{ini} and relative humidity conditions.

Impact of Thickness of Polymer Electrolyte Membrane and Gas Diffusion Layer on Temperature Distributions in Polymer Electrolyte Fuel Cell Operated at Temperature around 90 °C

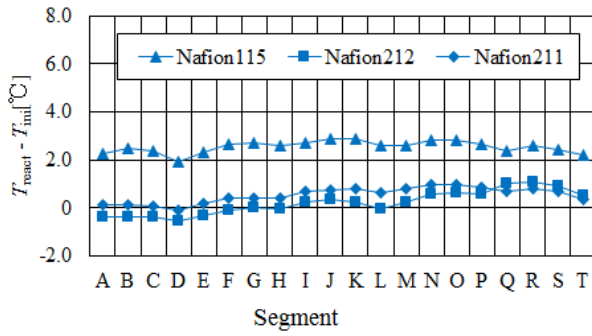
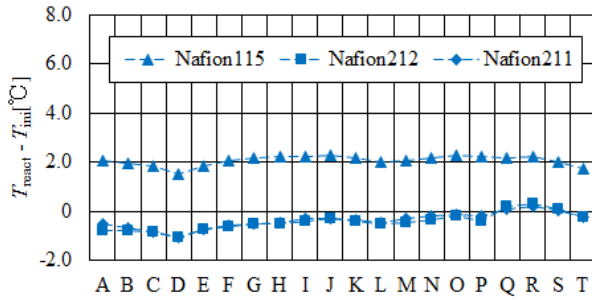
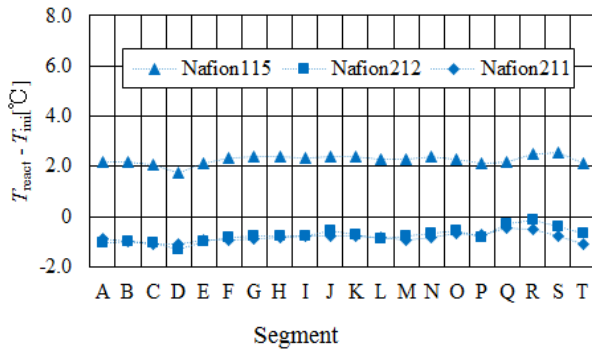
(a) $T_{ini} = 80 \text{ }^{\circ}\text{C}$ (b) $T_{ini} = 90 \text{ }^{\circ}\text{C}$ (c) $T_{ini} = 100 \text{ }^{\circ}\text{C}$

Fig. 17 Effect of thickness of PEM on T_{react} for A80%RH, C40%RH at $T_{ini} = 80 \text{ }^{\circ}\text{C}$, $90 \text{ }^{\circ}\text{C}$, $100 \text{ }^{\circ}\text{C}$ using TGP-H-030.

Since the thickness of Nafion 115 is the thickest among investigated PEMs, it is believed that the proton and water transfer is the worst among them [37]. Therefore, the power generation performance using Nafion 115 is also the worst which is shown in Table 3 and Figs. 19-21. It is known from Eqs. (1)-(3) that H_{react} is higher when W_E , i.e., the power generation performance, is smaller, resulting that T_{react} is higher according to Eq. (15). In addition, another reason might be that the condensation heat of accumulated water also

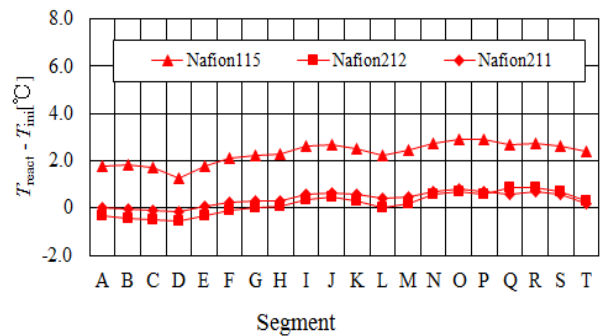
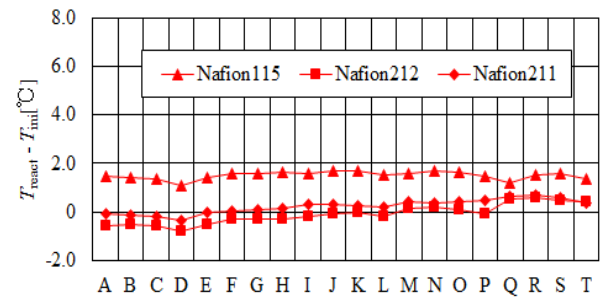
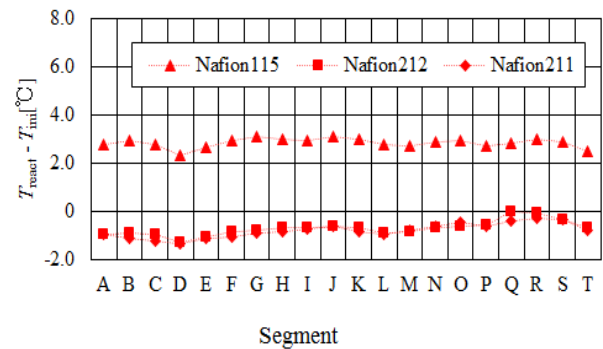
(a) $T_{ini} = 80 \text{ }^{\circ}\text{C}$ (b) $T_{ini} = 90 \text{ }^{\circ}\text{C}$ (c) $T_{ini} = 100 \text{ }^{\circ}\text{C}$

Fig. 18 Effect of thickness of PEM on T_{react} for A40%RH, C80%RH at $T_{ini} = 80 \text{ }^{\circ}\text{C}$, $90 \text{ }^{\circ}\text{C}$, $100 \text{ }^{\circ}\text{C}$ using TGP-H-030.

contributed to the rise of the temperature. On the other hand, it can be seen that the difference between the distribution of $T_{react} - T_{ini}$ using NRE-212 and that using NRE-211 is small except for A80%RH, C80%RH at $T_{ini} = 80 \text{ }^{\circ}\text{C}$ and $90 \text{ }^{\circ}\text{C}$. It is believed that water transfer is good with both NRE-212 and NRE-211 under low relative humidity or high operation temperature, e.g., $90 \text{ }^{\circ}\text{C}$ and $100 \text{ }^{\circ}\text{C}$, which results that the difference of the distribution of $T_{react} - T_{in}$ is not recognized well.

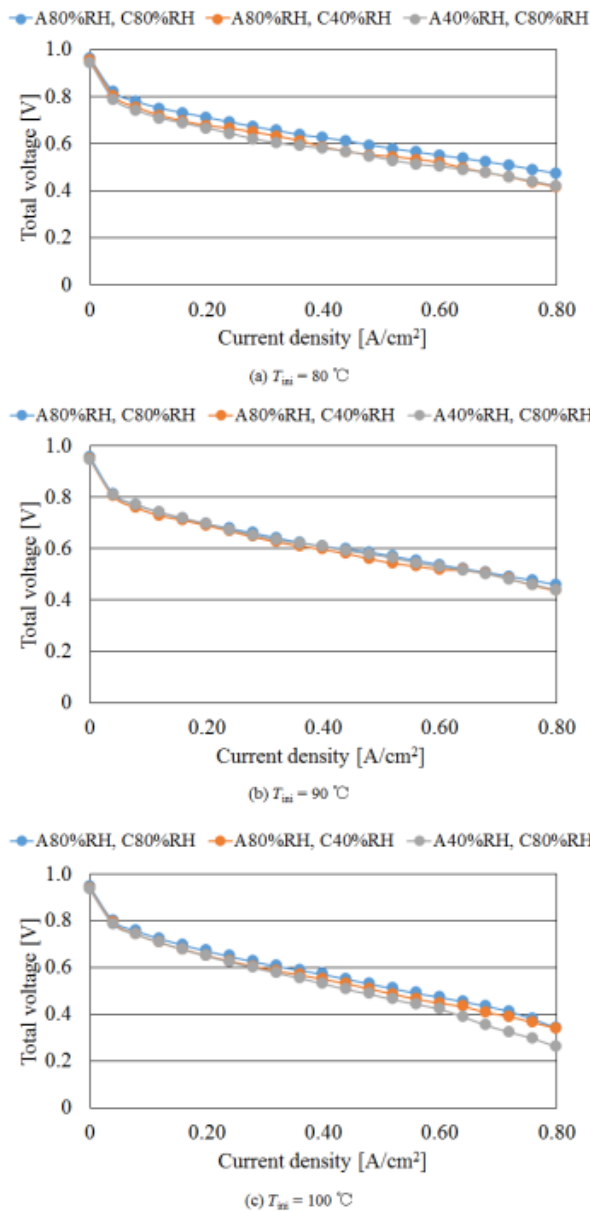


Fig. 19 Polarization curves in case of Nafion 115 & TGP-H-030 with different relative humidities and $T_{ini} = 80\text{ }^{\circ}\text{C}$, $90\text{ }^{\circ}\text{C}$, $100\text{ }^{\circ}\text{C}$, respectively.

However, it might be thought that the difference of water transfer between NRE-212 and NRE-211 due to the difference of thickness is larger under high relative humidity condition since liquid water is easy to be produced. Therefore, the difference between the distribution of $T_{react} - T_{ini}$ using NRE-212 and that using NRE-211 is relatively large for A80%RH, C80%RH at $T_{ini} = 80\text{ }^{\circ}\text{C}$ and $90\text{ }^{\circ}\text{C}$. In other words, it can be claimed that $T_{react} - T_{ini}$ is increased from the

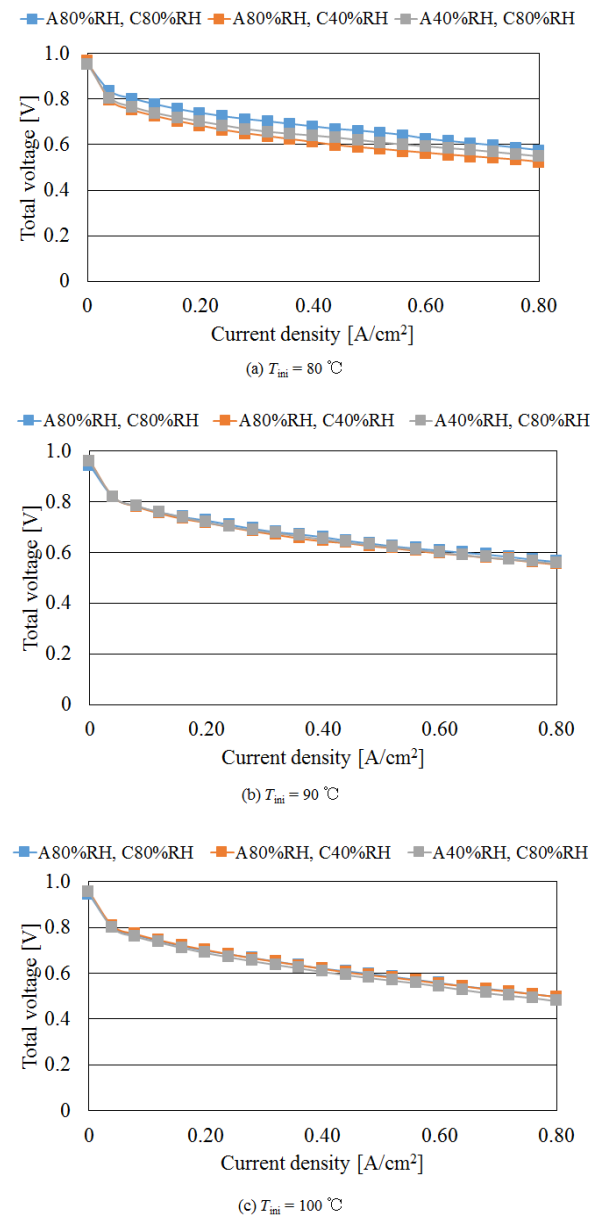


Fig. 20 Polarization curves in case of NRE-212 & TGP-H-030 with different relative humidities and $T_{ini} = 80\text{ }^{\circ}\text{C}$, $90\text{ }^{\circ}\text{C}$, $100\text{ }^{\circ}\text{C}$, respectively.

inlet to the outlet using NRE-212, which is the same as the case using TGP-H-060 as shown before, due to the bad water transfer performance relatively.

After the investigation among all operation conditions, it is revealed that the even temperature distribution and high power generation performance with operation temperature around $90\text{ }^{\circ}\text{C}$ could be obtained if using NRE-211 and TGP-H-030. Though this study reveals the combination of NRE-211 and

Table 3 Data of power generation experiment.

PEM	T_{ini} [°C]	Relative humidity of supply gas	Voltage [V]
Nafion 115	80	A80%RH, C80%RH	0.48
		A80%RH, C40%RH	0.44
		A40%RH, C80%RH	0.45
	90	A80%RH, C80%RH	0.47
		A80%RH, C40%RH	0.45
		A40%RH, C80%RH	0.45
	100	A80%RH, C80%RH	0.35
		A80%RH, C40%RH	0.34
		A40%RH, C80%RH	0.25
NRE-212	80	A80%RH, C80%RH	0.62
		A80%RH, C40%RH	0.60
		A40%RH, C80%RH	0.60
	90	A80%RH, C80%RH	0.58
		A80%RH, C40%RH	0.58
		A40%RH, C80%RH	0.57
	100	A80%RH, C80%RH	0.51
		A80%RH, C40%RH	0.51
		A40%RH, C80%RH	0.50
NRE-211	80	A80%RH, C80%RH	0.57
		A80%RH, C40%RH	0.58
		A40%RH, C80%RH	0.58
	90	A80%RH, C80%RH	0.59
		A80%RH, C40%RH	0.63
		A40%RH, C80%RH	0.60
	100	A80%RH, C80%RH	0.54
		A80%RH, C40%RH	0.54
		A40%RH, C80%RH	0.53

TGP-H-030 is effective at operation temperature around 90 °C, another optimum thickness would exist if the thinner PEM and GDL were used.

4. Conclusions

The temperature distribution on reaction surface was calculated by the 1D multi-plate heat transfer model proposed by this study under operation temperature around 90 °C condition. This study focused on the investigation of the impact of thicknesses of PEM and GDL on temperature distribution on reaction surface among different T_{ini} , flow rate, relative humidity of supply gas. As a result, the following conclusions have been drawn:

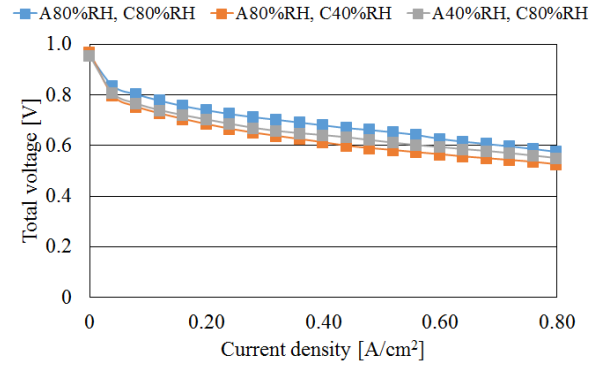
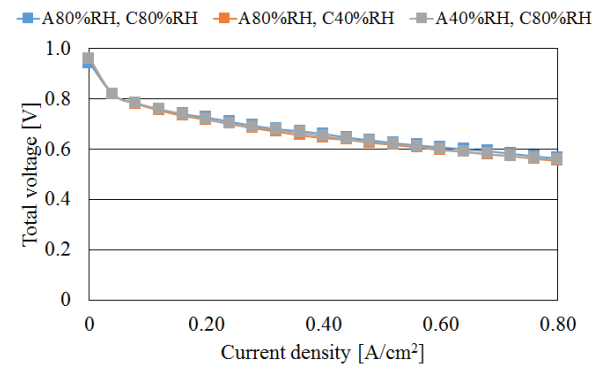
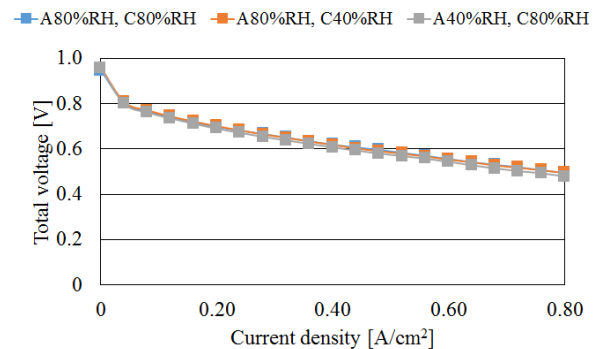
(a) $T_{ini} = 80$ °C(b) $T_{ini} = 90$ °C(c) $T_{ini} = 100$ °C

Fig. 21 Polarization curves in case of NRE-211 & TGP-H-030 with different relative humidities and $T_{ini} = 80$ °C, 90 °C, 100 °C, respectively.

The impact of flow rate of supply gas at the inlet on the temperature distribution is not significant. When using thin GDL, the power generation is performed from the inlet to the outlet uniformly due to good gas diffusion, resulting in the even distribution of $T_{react} - T_{ini}$ irrespective of the thickness of PEM, the T_{ini} and the relative humidity. It can be clarified that the thin GDL is effective for controlling the heat and mass transfer at higher temperature. It is also revealed that

$T_{\text{react}} - T_{\text{ini}}$ using Nafion 115 is higher than the other PEMs irrespective of T_{ini} and relative humidity conditions since the proton and water transfer is the worst among them due to the thickest thickness among investigated PEMs. The study proves that the difference between the distribution of $T_{\text{react}} - T_{\text{ini}}$ with NRE-212 and that with NRE-211 is small except for the conditions under which liquid water is easy to be produced. Finally, it can conclude that the even temperature distribution and high power generation process with operation temperature around 90 °C could be obtained if NRE-211 and TGP-H-030, i.e., with thin PEM and GDL being used.

Acknowledgments

This work was supported by Mie prefecture industrial research institute as well as Mie industry and enterprise support center. The authors acknowledge their great contribution.

References

- [1] NEDO (New Energy and Industry Technology Development Organization), <http://www.nedo.go.jp/content/100871973.pdf>.
- [2] Zhang, G., and Kandlikar, S. G. 2012. "A Critical Review of Cooling Technique in Proton Exchange Membrane Fuel Cell Stacks." *International Journal of Hydrogen Energy* 37 (February): 2412-29.
- [3] Agbossou, K., Kolhe, M., Hamelin, J., and Bose, T. K. 2004. "Performance of a Stand-Alone Renewable Energy System Based on Energy Storage as Hydrogen." *IEEE Transactions on Energy Conversion* 19 (October): 633-40.
- [4] Li, Q., He, R., Jensen, J. O., and Bjerrum, N. J. 2003. "Approaches and Recent Development Polymer Electrolyte Membrane for Fuel Cells Operating above 100 °C." *Chemical of Materials* 15 (26): 4896-915.
- [5] Chen, C. Y., and Su, S. C. 2018. "Development and Performance Evaluation of a High Temperature Proton Exchange Membrane Fuel Cell with Stamped 304 Stainless Steel Bipolar Plates." *International Journal of Hydrogen Energy* 4: 13430-9.
- [6] Devrim, Y., Arica, E. D., and Albostan, A. 2018. "Graphene Based Catalyst Supports for High Temperature PEM Fuel Cell Application." *International Journal of Hydrogen Energy* 4: 11820-9.
- [7] Kannan, A., Kaczeriwski, J., Kabza, A., and Sholta, J. 2018. "Operation Strategies Based on Carbon Corrosion and Lifetime Investigations for High Temperature Polymer Electrolyte Membrane Fuel Cell Stacks." *Fuel Cells* 3: 287-98.
- [8] Nalbant, Y., Colpan, C. O., and Derim, Y. 2018. "Development of a One-Dimensional and Semi-Empirical Model for a High Temperature Proton Exchange Membrane Fuel Cell." *International Journal of Hydrogen Energy* 43: 5939-50.
- [9] Zhang, Q., Ling, Y., Cai, W., Yu, X., and Yang, Z. 2017. "High Performance and Durability of Polymer-Coated Pt Electrocatalyst Supported on Oxidized Multi-walled in High-Temperature Polymer Electrolyte Fuel Cells." *International Journal of Hydrogen Energy* 42: 16714-21.
- [10] Quartarone, E., Angioni, S., and Mustarelli, P. 2017. "Polymer and Composite Membranes for Proton-Conducting, High-Temperature Fuel Cells: A Critical Review." *Materials* 10 (687): 1-17.
- [11] Thomas, S., Vang, J. R., Araya, S. S., and Kar, S. K. 2017. "Experimental Study to Distinguish the Effects of Methanol Slip and Water Vapour on a High Temperature PEM Fuel Cell at Different Operating Conditions." *Applied Energy* 192: 422-36.
- [12] Rasheed, R. K. A., Liao, Q., Caizhi, Z., and Chan, S. H. 2017. "A Review on Modeling of High Temperature Proton Exchange Membrane Fuel Cells (HT-PEMFCs)." *International Journal of Hydrogen Energy* 42: 3142-65.
- [13] Rosli, R. E., Sulong, A. B., Daud, W. A. R., Zulkifley, M. A., Husaini, T., Rosli, M. I. Majlan, E. H., and Haque, M. M. 2017. "A Review of High-temperature Proton Exchange Membrane Fuel Cell (HT-PEMFC) System." *International Journal of Hydrogen Energy* 42: 9293-314.
- [14] Lee, D., Lim, J. W., and Lee, D. G. 2017. "Cathode/Anode Integrated Composite Bipolar Plate for High-Temperature PEMFC." *Composite Structures* 167: 144-51.
- [15] Singdeo, D., Dey T., Gaikwad, S., Andreasen, S. J., and Ghosh, P. C. 2017. "A New Modified-serpentine Flow Field for Application in High Temperature Polymer Electrolyte Fuel Cell." *Applied Energy* 195: 13-22.
- [16] Lakshmi, R. B., Harikrishnan, N. P., and Juliet, A. V. 2017. "Comparative Analysis of 2D and 3D Model of a PEMFC in COSOL." *Applied Surface Science* 418: 99-102.
- [17] Lee, C.-Y., Chiang, Y.-C., Weng, F.-B., Li, S.-C., Wu, P.-H., and Yueh, H.-I. 2017. "Flexible Micro Temperature, Voltage and Current Sensors for Local Real-time Microscopic Diagnosis inside High Temperature Proton Exchange Membrane Fuel Cell Stack." *Renewable Energy* 108: 126-31.
- [18] Haque, M. A., Sulong, A. B., Loh, K. S., Majlan, E. H., Husaini, T., and Rosli, R. E. 2017. "Acid Doped

- Polybenzimidazoles Based Membrane Electrode Assembly for High Temperature Proton Exchange Membrane Fuel Cell: A Review.” *International Journal of Hydrogen Energy* 42: 9156-79.
- [19] Rasheed, R. K. A., Zhang, C., and Chan, S. H. 2017. “Numerical Analysis of High-Temperature Proton Exchange Membrane Fuel Cells during Start-up by Inlet Gas Heating and Applied Voltage.” *International Journal of Hydrogen Energy* 42: 10390-406.
- [20] Lee, C.-Y., Weng, F.-B., Kuo, Y.-W., Tsai, C.-H., Cheng, Y.-T., Cheng, C.-K., and Lin, J.-T. 2016. “In-situ Measurement of High-Temperature Proton Exchange Membrane Fuel Cell Stack Using Flexible Five-in-One Micro-sensors.” *Sensors* 16 (1731): 1-10.
- [21] Kim, H. S., Jeon, S. W., Cha, D., and Kim, Y. 2016. “Numerical Analysis of a High-Temperature Proton Exchange Membrane Fuel Cell under Humidified Operation with Stepwise Reactant Supply.” *International Journal of Hydrogen Energy* 41: 13657-65.
- [22] Zhang, C., Yu, T., Yi, J., Liu, Z., Raj, K. A. R., Xia, L., Tu, Z., and Chan, S. H. 2016. “Investigation of Heating and Cooling in a Stand-Alone High Temperature PEM Fuel Cell System.” *Energy Conversion and Management* 129: 36-42.
- [23] Araya, S. S., Zhou, F., Liso, V., Sahlin, S. L., Vang, J. R., Thomas, S., Gao, X., Jeppesen, C., and Kar, S. K. 2016. “A Comprehensive Review of PBI-Based High Temperature PEM Fuel Cells.” *International Journal of Hydrogen Energy* 41: 21310-44.
- [24] Reimer, U., Ehlert, J., Janssen, H., and Lehnert, W. 2016. “Water Distribution in High Temperature Polymer Electrolyte Fuel Cells.” *International Journal of Hydrogen Energy* 41: 1837-45.
- [25] Waller, M. G., Walluk, M. R., and Trabold, T., A. 2016. “Performance of High Temperature PEM Fuel Cell Materials. Part 1: Effects of Temperature, Pressure and Anode Dilution.” *International Journal of Hydrogen Energy* 41: 2944-54.
- [26] Caglayan, D. G., Sezgin, B., Devrim, Y., and Eroglu, I. 2016. “Three-dimensional Modeling of a High Temperature Polymer Electrolyte Membrane Fuel Cell at Different Operation Temperatures.” *International Journal of Hydrogen Energy* 41: 10060-70.
- [27] Jheng, L.-C., Chang, W. J.-Y., Hsu, S. L.-C., and Cheng, P.-Y. 2016. “Durability of Symmetrically and Asymmetrically Porous Polybenzimidazole Membranes for High Temperature Proton Exchange Membrane Fuel Cells.” *Journal of Power Sources* 323: 57-66.
- [28] Rasheed, R. K. A., and Chan, S. H. 2016. “Analysis of Steady State Heating Configuration for High-Temperature Proton Exchange Membrane Fuel Cell Based on Multi-physical Numerical Modeling.” *Electrochimica Acta* 222: 280-92.
- [29] Nishimura, A., Shibuya, K., Morimoto, A., Tanaka, S., Hirota, M., Nakamura, Y., Kojima, M., Narita, M., and Hu, E. 2012. “Dominant Factor and Mechanism of Coupling Phenomena in Single Cell of Polymer Electrolyte Fuel Cell.” *Applied Energy* 90 (1): 73-9.
- [30] Nishimura, A., Iio, K., Baba, M., Yamauchi, T., Hirota, M., and Hu, E. 2014. “Modeling of Heat Transfer in Single Cell of Polymer Electrolyte Fuel Cell by Means of Temperature Data Measured by Thermograph.” *Journal of Chemical Engineering of Japan* 47 (7): 521-9.
- [31] Nishimura, A., Fukuoka, T., Baba, M., Hirota, M., and Hu, E. 2015. “Clarification on Temperature Distribution in Single Cell of Polymer Electrolyte Fuel Cell under Different Operation Conditions by Means of 1D Multi-plate Heat-Transfer Model.” *Journal of Chemical Engineering of Japan* 48 (10): 862-71.
- [32] Nishimura, A., Osada, K., Tsunoda, T., Yoshimura, M., Hirota, M., and Hu, E. 2016. “Analysis on Temperature Distributions in Single Cell of Polymer Electrolyte Fuel Cell when Operated in High Temperature Range.” *Journal of Energy and Power Engineering* 10: 453-64.
- [33] Khandelwal, M., and Mench, M. M. 2006. “Direct Measurement of Through-Plane Thermal Conductivity and Contact Resistance in Fuel Cell Materials.” *Journal of Power Sources* 161 (2): 1106-15.
- [34] Kawase, M., Inagaki, T., Kawashima, S., and Miura, K. 2009. “Effective Thermal Conductivity of Gas Diffusion Layer in Through-Plane Direction.” *ECS Transactions* 25 (1): 1529-37.
- [35] Jung, C. Y., Shim, H. S., Koo, S. M., Lee, S. H., and Yi, S. C. 2012. “Investigation of the Temperature Distribution in Proton Exchange Membrane Fuel Cell.” *Applied Energy* 93 (May): 733-41.
- [36] Nishimura, A., Zamami, K. P., Yoshimoto, M., Hirota, M., and Kolhe, M. L. 2017. “Numerical Analysis of Temperature Distributions in Single Cell of Polymer Electrolyte Fuel Cell when Operated in Elevated Temperature Range.” *Journal of Energy and Power Engineering* 11: 193-408.
- [37] Penga, Z., Tolj, I., and Barbir, F. 2016. “Computational Fluid Dynamics Study of PEM Fuel Cell Performance for Isothermal and Non-uniform Temperature Boundary Conditions.” *International Journal of Hydrogen Energy* 41: 17585-94.
- [38] Cooper, N. J., Santamaria, A. D., Becton, M. K., and Park, J. W. 2017. “Neutron Radiography Measurements of In-Situ PEMFC Liquid Water Saturation in 2D & 3D Morphology Gas Diffusion Layers.” *International Journal of Hydrogen Energy* 42: 16269-78.
- [39] Nishimura, A., Sato, Y., Yoshimura, M., Kamiya, S., and Hirota, M. 2018. “Impact of Thickness of Polymer

Electrolyte Membrane on Temperature Distributions in Single Cell of Polymer Electrolyte Fuel Cell Operated at High Temperature.” *Journal of Energy and Power Engineering* 12: 80-92.

- [40] Alizadeh, E., Rahmi-Esbo, M., Rahgoshay, S. M., and Saadat, S. H. M. 2017. “Numerical and Experimental Investigation of Cascade Type Serpentine Flow Field of Reactant Gases for Improving Performance of PEM Fuel Cell.” *International Journal of Hydrogen Energy* 42: 14708-24.
- [41] Rahimi-Ebso, M., Ranjbar, A. A., Ramiar, A., Alizadeh, E., and Aghaee, M. 2016. “Improving PRM Fuel Cell Performance and Effective Water Removal by Using a Novel Gas Flow Field.” *International Journal of Hydrogen Energy* 41: 3023-37.
- [42] The Japan Society of Mechanical Engineers. 1993. *JSME Heat Transfer Handbook*. Maruzen, Tokyo.
- [43] Hwang, S. S., Han, S. S., Lee, P. H., and Park, B. I. 2010. “Transient Performance Behavior of Proton Exchange Membrane Fuel Cell by Configuration of Membrane and Gas Diffusion Layer.” *Journal of Thermal Science and Technology* 5 (1): 165-77.
- [44] Toray Corp, http://www.torayca.com/properties/en/images/report_eng09_2.html; 2019.